Sumner, E.J.; Peakall, J.; Dorrell, R.M.; Parsons, D.R.; Darby, S.E.; Wynn, R.B.; McPhail, S.D.; Perrett, J.; Webb, A.; White, D.. 2014 Driven around the bend: Spatial evolution and controls on the orientation of helical bend flow in a natural submarine gravity current. *Journal of Geophysical Research: Oceans*, 119 (2). 898-913. 10.1002/2013JC009008

Sumner, E.J.; Peakall, J.; Dorrell, R.M.; Parsons, D.R.; Darby, S.E.; Wynn, R.B.; McPhail, S.D.; Perrett, J.; Webb, A.; White, D.. 2014 Driven around the bend: Spatial evolution and controls on the orientation of helical bend flow in a natural submarine gravity current. *Journal of Geophysical Research: Oceans*, 119 (2). 898-913. 10.1002/2013JC009008

AGU PUBLICATIONS

JGR

Journal of Geophysical Research: Oceans

RESEARCH ARTICLE

10.1002/2013JC009008

Key Points:
- First data of the 3-D velocity and density structure of a submarine gravity flow
- Internal pressure gradients, not centrifugal forces control flow structure
- Flow stratification and downstream advection must be included in future models

Correspondence to:
E. J. Sumner,
e.j.sumner@soton.ac.uk

Citation:
Sumner, E. J., J. Peakall, R. M. Dorrell, D. R. Parsons, S. E. Darby, R. B. Wynn, S. D. McPhail, J. Perrett, A. Webb, and D. White (2014), Driven around the bend: Spatial evolution and controls on the orientation of helical bend flow in a natural submarine gravity current, *J. Geophys. Res. Oceans*, *119*, 898–913, doi:10.1002/2013JC009008.

Received 7 APR 2013
Accepted 10 JAN 2014
Accepted article online 16 JAN 2014
Published online 12 FEB 2014

Driven around the bend: Spatial evolution and controls on the orientation of helical bend flow in a natural submarine gravity current

E. J. Sumner[1,2], J. Peakall[3], R. M. Dorrell[3], D. R. Parsons[4], S. E. Darby[5], R. B. Wynn[6], S. D. McPhail[6], J. Perrett[6], A. Webb[6], and D. White[6]

[1]Ocean and Earth Science, University of Southampton, Southampton, UK, [2]Monterey Bay Aquarium Research Institute, Moss Landing, California, USA, [3]School of Earth and Environment, University of Leeds, Leeds, UK, [4]Department of Geography, Environment and Earth Sciences, University of Hull, UK, [5]Geography and Environment, University of Southampton, Southampton, UK, [6]National Oceanography Centre, Southampton, UK

Abstract Submarine channel systems transport vast amounts of terrestrial sediment into the deep sea. Understanding the dynamics of the gravity currents that create these systems, and in particular, how these flows interact with and form bends, is fundamental to predicting system architecture and evolution. Bend flow is characterized by a helical structure and in rivers typically comprises inwardly directed near-bed flow and outwardly directed near-surface flow. Following a decade of debate, it is now accepted that helical flow in submarine channel bends can exhibit a variety of structures including being opposed to that observed in rivers. The new challenge is to understand what controls the orientation of helical flow cells within submarine flows and determines the conditions for reversal. We present data from the Black Sea showing, for the first time, the three-dimensional velocity and density structure of an active submarine gravity current. By calculating the forces acting on the flow, we evaluate what controls the orientation of helical flow cells. We demonstrate that radial pressure gradients caused by across-channel stratification of the flow are more important than centrifugal acceleration in controlling the orientation of helical flow. We also demonstrate that nonlocal acceleration of the flow due to topographic forcing and downstream advection of the cross-stream flow are significant terms in the momentum balance. These findings have major implications for conceptual and numerical models of submarine channel dynamics, because they show that three-dimensional models that incorporate across-channel flow stratification are required to accurately represent curvature-induced helical flow in such systems.

1. Introduction

Submarine channel systems are major morphological features on the ocean floor that enable terrestrial sediment to be transported hundreds, or even thousands of kilometers from the continental shelf into the deep sea [*Wynn et al*., 2007]. The submarine gravity currents (e.g., turbidity currents) responsible for forming these channel systems have proven extremely difficult to monitor directly due to their inaccessible location, infrequent occurrence, and their often destructive nature [*Khripounoff et al*., 2003; *Paull et al*., 2003; *Xu and Noble*, 2004; *Xu et al*., 2013; *Talling et al*., 2012]. However, understanding the dynamics of these flows is important. Submarine gravity currents pose a significant hazard to seafloor infrastructure such as internet cables and oil pipelines. They transport sediment, organic material, and pollutants around the Earth's surface, thereby playing an important though poorly understood role in global biogeochemical cycles. The sediment routed through submarine channel systems ultimately forms submarine fans, which are some of the largest sedimentary bodies on Earth [*Emmel and Curray*, 1983] and which can contain valuable hydrocarbon reserves [e.g., *Mayall et al*., 2006; *Babonneau et al*., 2010]. A better understanding of the three-dimensional flow fields in submarine channels is therefore fundamental to understanding and predicting their sedimentary architecture and how such systems evolve both spatially and temporally.

There are many similarities between the morphology of submarine and subaerial channel systems and this has led to arguments regarding how similar the flow and morphodynamics of these two systems are [*Peakall et al*., 2000]. It is well understood that flow around river bends is characterized by a helical structure that results from local imbalances in the radial forces acting on the flow [e.g., *Rozovskii*, 1957; *Dietrich and Smith*,

1983; *Thorne et al*., 1985]. Importantly, the nature of the helical flow structure is fundamental in determining the spatial pattern of boundary stress within bends, thereby controlling where sediment is eroded, transported, and deposited around the bend and therefore how the channel system evolves. Fierce debate over the last decade has led to the conclusion that helical flow in submarine channel bends can behave differently to that in rivers and that it can display a variety of complex structures [*Kassem and Imran*, 2004; *Corney et al*., 2006, 2008; *Keevil et al*., 2006, 2007; *Abad et al*., 2011; *Giorgio Serchi et al*., 2011; *Huang et al*., 2012; *Janocko et al*., 2013; *Dorrell et al*., 2013]. Recently, the debate has started to move on, with a limited number of theoretical studies [*Abad et al*., 2011; *Dorrell et al*., 2013] exploring the fundamental controls on the orientation of helical flow cells and therefore how common different helical flow structures actually are. These studies are extremely valuable, however, such theoretical approaches are fundamentally constrained by a lack of field data. In this study, we present the first field data showing how the three-dimensional velocity and density structure within an active channelized submarine gravity current evolves as the flow travels around a bend. Importantly, the field data are sufficiently detailed to resolve the radial force balance governing the helical structure of the flow and therefore its spatial and temporal development. The results so obtained provide unprecedented insight into the dynamics of a natural channelized submarine gravity current with implications for the future development of conceptual, numerical, and experimental models of these flows.

1.1. Helical Flow

As fluid flows travel around bends, curvature-induced centrifugal acceleration forces the fluid to move outward, resulting in a superelevation of fluid at the outer bank, which in turn sets up a radial pressure field, typically directed toward the inner bank. The outward-directed centrifugal and inward-directed pressure gradient forces are locally imbalanced within the vertical. This typically results in a cross-stream circulation cell, in which near-surface fluid moves toward the outer bank and near-bed fluid moves toward the inner bank [e.g., *Rosovskii*, 1957; *Thorne et al*., 1985]. Downstream advection of these cross-stream flow structures results in an overall helical flow structure.

There are many similarities between subaerial channel systems and submarine channel systems, for example their gross planform morphology and smaller scale features such as crevasse splays and point bars [*Klaucke and Hesse*, 1996; *Peakall et al*., 2000, 2007; *Kolla et al*., 2007] but it is unclear whether subaerial and submarine channel systems develop and evolve through similar processes [e.g., *Pirmez and Imran*, 2003]. It is important to note, that there are fundamental differences between the fluid flows that create subaerial and submarine channel systems, which might suggest significant differences also exist between the dynamics of these two systems. Open-channel flows and submarine density currents have very different vertical profiles of the primary flow velocity, with the location of the velocity maximum generally being located toward the surface in open-channel flows, but toward the base of density currents [e.g., *Garcia and Parker*, 1989; *Peakall et al*., 2000; *Felix*, 2002; *Manica*, 2012]. Open-channel flows tend to be well confined by their channel systems, whereas density currents may be unconfined, with the potential for material to be lost from the flow through processes such as flow stripping [*Piper and Normark*, 1983; *Peakall et al*., 2000]. The density contrast between the flow and the surrounding ambient fluid is much less for submarine density currents than it is for open-channel flows, which is likely to affect the degree of superelevation of the flow at the outer bend and therefore lateral pressure gradients within the flow [*Komar*, 1969; *Dorrell et al*., 2013]. The lateral pressure gradients may also be modified within submarine gravity currents due to lateral flow stratification [e.g., *Kassem and Imran*, 2004; *Giorgio Serchi*, 2011; *Janocko et al*., 2013]. The larger scale of some submarine channel systems also means that Coriolis forces resulting from the Earth's rotation can potentially also be important [*Cossu and Wells*, 2010, 2013; *Dorrell et al*., 2013; *Peakall et al*., 2013].

Initial numerical investigations [*Imran et al*., 1999; *Kassem and Imran*, 2004] of helical flow in submarine channel bends suggested that such bends exhibit a similar helical flow structure to rivers. However, these results were apparently contradicted by numerical and experimental studies [*Corney et al*., 2006; *Keevil et al*., 2006], which demonstrated that gravity currents flowing around bends could exhibit helical circulation with the opposite sense of rotation to river flows (river-reversed), i.e., with near-bed flow at the bend apex directed toward the outer bend and near-surface flow directed toward the inside of the bend.

Subsequently, a variety of studies including numerical and experimental models [*Keevil et al*., 2007; *Corney et al*., 2008; *Islam and Imran*, 2008; *Cossu and Wells*, 2010; *Abad et al*., 2011; *Giorgio Serchi et al*., 2011; *Huang*

et al., 2012; *Mahdinia et al*., 2012; *Janocko et al*., 2013], measurements of field-scale submarine density currents [*Parsons et al*., 2010], and examination of ancient deposits in the rock record [*Pyles et al*., 2012] have demonstrated the occurrence of both river-like and river-reversed helical flows in submarine channel bends as well as the occurrence of multiple vertically stacked helical flow cells [e.g., *Rosovskii*, 1957; *Imran et al*., 2007; *Islam and Imran*, 2008; *Giorgio Serchi et al*., 2011]. Having established that a variety of helical flow patterns are possible, the debate has now moved on to understanding what controls the orientation of helical flow in submarine density currents and therefore how common different modes of helical circulation are in natural systems [*Abad et al*., 2011; *Giorgio Serchi et al*., 2011] and examining the implications of such reversals for channel morphology [*Peakall et al*., 2007; *Amos et al*., 2010; *Darby and Peakall*, 2012; *Janocko et al*., 2013].

Corney et al. [2008] combined experiments with numerical modeling to suggest that the orientation of helical flow cells is controlled by the vertical position of the velocity maximum, with helical flow being river-like when the velocity maximum is located high up in the flow, but reversed when the velocity maximum is near the bed. They suggest that the position of the downstream velocity maximum in most density currents will be sufficiently close to the flow bed that secondary flow is likely reversed. *Abad et al*. [2011] combined theory, experiments, and reconstructions of flows based on field data to suggest that flows are likely to be reversed when densimetric Froude number is either high with a near-bed velocity maximum, or densimetric Froude number is low with low boundary drag. They suggested that under most circumstances likely to occur in natural submarine density currents helical flow will be river-like. *Giorgio Serchi et al*. [2011] used a 3-D numerical model to investigate the orientation of helical flow cells for saline density currents on variable slopes. They concurred with *Corney et al*. [2008] that the orientation of helical flow cells relates to the height of the velocity maximum, but in addition they demonstrated that baroclinic forces caused by tilting of isopycnals within the flow are also an important control on the orientation of helical flow cells.

Recent field studies of helical flow in curved stratified estuaries [e.g., *Seim and Gregg*, 1997; *Lacy and Monismith*, 2001; *Nidzieko et al*., 2009] and oceanographic straits [*Umlauf et al*., 2007; *Umlauf and Arneborg*, 2009a, 2009b; *Fer et al*., 2010] provide a wealth of complementary information. Helical flow in curved estuaries may be river-like [*Geyer*, 1993; *Seim and Gregg*, 1997; *Nidzieko et al*., 2009], river-reversed [*Chant and Wilson*, 1997; *Seim and Gregg*, 1997; *Lacy and Monismith*, 2001; *Nidzieko et al*., 2009], or comprise multiple stacked flow cells [*Cheng et al*., 2009; *Nidzieko et al*., 2009]. River-reversed helical flow and multiple flow cells occur in highly stratified estuaries and result from strong baroclinic pressure gradients caused by lateral salinity gradients [*Lacy and Monismith*, 2001; *Nidzieko et al*., 2009]. In general, baroclinic pressure gradients are found to oppose centrifugal forcing causing the river-like helical flow to weaken and be replaced by a reversed helical flow cell [*Nidzieko et al*., 2009]. As elucidated in section 1.2, the orientation and structure of the helical circulation is likely controlled by the balance between centrifugal and baroclinic forces and also the variable response time of the flow to these different forces [*Nidzieko et al*., 2009].

1.2. Governing Equations for a Submarine Gravity Current

In this paper, we analyze the flow using a coordinate system in which the θ axis is oriented along the channel centerline (with positive values downstream), the r axis is perpendicular to the θ axis (positive oriented toward the right-hand bank looking downstream) and the z axis is oriented vertically upward. Following the Boussinesq approximation, where suspended sediment concentration is assumed dilute [*Meiburg and Kneller*, 2010], the Reynolds averaged mass and momentum equations can be written as

Mass conservation (fluid):

$$\frac{1}{r}\frac{\partial r u_r}{\partial r}+\frac{1}{r}\frac{\partial u_\theta}{\partial \theta}+\frac{\partial u_z}{\partial z}=0 \tag{1}$$

Momentum conservation (fluid):

$$\underbrace{\frac{\partial u_r}{\partial t}}_{\text{temporal acceleration}}+\underbrace{u_r\frac{\partial u_r}{\partial r}+\frac{u_\theta}{r}\frac{\partial u_r}{\partial \theta}+u_z\frac{\partial u_r}{\partial z}}_{\text{convective acceleration}}\underbrace{-\frac{u_\theta^2}{r}}_{\text{centrifugal acceleration}}=\underbrace{-\frac{1}{\rho_\omega}\frac{\partial P}{\partial r}}_{\text{pressure gradient}}+\underbrace{f u_\theta}_{\text{Coriolis}}\underbrace{-\frac{1}{\rho_\omega}\left(\frac{\partial \tau_{rr}}{\partial r}+\frac{1}{r}\frac{\partial \tau_{r\theta}}{\partial \theta}+\frac{\partial \tau_{rz}}{\partial z}\right)}_{\text{summed Reynolds stresses}} \tag{2}$$

$$\underbrace{\frac{\partial u_\theta}{\partial t}}_{\text{temporal acceleration}} + \underbrace{u_r \frac{\partial u_\theta}{\partial r} + \frac{u_\theta}{r}\frac{\partial u_\theta}{\partial \theta} + u_z \frac{\partial u_\theta}{\partial z}}_{\text{convective acceleration}} + \underbrace{\frac{u_r u_\theta}{r}}_{\text{angular acceleration}} = \underbrace{-\frac{1}{\rho_\omega}\frac{\partial P}{\partial \theta}}_{\text{pressure gradient}} \underbrace{-f u_r}_{\text{Coriolis}} - \frac{1}{\rho_\omega}\underbrace{\left(\frac{\partial \tau_{\theta r}}{\partial r} + \frac{1}{r}\frac{\partial \tau_{\theta\theta}}{\partial \theta} + \frac{\partial \tau_{\theta z}}{\partial z}\right)}_{\text{summed Reynolds stresses}} \quad (3)$$

$$\underbrace{\frac{\partial u_z}{\partial t}}_{\text{temporal acceleration}} + \underbrace{u_r \frac{\partial u_z}{\partial r} + \frac{u_\theta}{r}\frac{\partial u_z}{\partial \theta} + u_z \frac{\partial u_z}{\partial z}}_{\text{convective acceleration}} = -\frac{1}{\rho_\omega}\frac{\partial P}{\partial z} + \underbrace{g\,\Phi\left(\frac{\rho_s}{\rho_\omega} - 1\right)}_{\text{pressure gradient}} - \frac{1}{\rho_\omega}\underbrace{\left(\frac{\partial \tau_{zr}}{\partial r} + \frac{1}{r}\frac{\partial \tau_{z\theta}}{\partial \theta} + \frac{\partial \tau_{zz}}{\partial z}\right)}_{\text{summed Reynolds stresses}} \quad (4)$$

where t denotes the time coordinate, u the flow velocity (where subscripts θ, r, and z denote the three components of velocity defined above), ρ_ω the density of the ambient fluid, P pressure, g gravitational acceleration, Φ the excess concentration of the flow relative to the ambient fluid, f the Coriolis parameter, and the matrix τ represents the summed viscous and Reynolds stresses. From the above, the density of the flow ρ_f may be defined as:

$$\rho_{f=}\ \rho_\omega + \rho_s \phi \quad (5)$$

where ρ_s denotes the density of the material transported by the flow.

In principle, equations (1–5) provide a complete and precise description of flow within a submarine gravity current, and as such the flow field is seen to be governed by a complex balance between the inertial, convective, Coriolis, and pressure gradient forces, as well as the viscous and turbulent stresses. However, in practice it is not feasible to acquire all the synoptic measurements to close these governing equations. As such, in practical applications, additional assumptions are introduced in order to simplify the equations to the point at which a solution becomes tractable.

In this study, we employ the shallow water form of the above governing equations. In the shallow water derivation, it is assumed that the vertical scale is of the order of the flow depth (H) and is much smaller than the horizontal length scale (L), such that the aspect ratio $\delta = H/L << 1$. It is further assumed that the radial velocity along a line of constant curvature is small in relation to the streamwise velocity, and therefore, from fluid mass conservation that the vertical velocity component is small in relation to the radial velocity, i.e.,

$$u_z = O(\delta) u_r = O\left(\delta^2\right) u_\theta \quad (6)$$

Note that this assumption implies that the bend is well defined by a circular arc, which may not be the case in natural systems. Furthermore, applying the above scaling arguments to the vertical momentum equation (4) implies that the flow is hydrostatic to leading order:

$$\frac{1}{\rho_\omega}\frac{\partial P}{\partial z} = g\Phi\left(\frac{\rho_s}{\rho_\omega} - 1\right) + O(\delta) \quad (7)$$

Assuming that the flow is submerged in an infinitely deep fluid and that the pressure tends to a constant, P_a, as $z \to \infty$, the hydrostatic pressure field of the flow is:

$$P = P_a + \rho_\omega g\left(\frac{\rho_s}{\rho_\omega} - 1\right)\int_z^\infty \Phi dz' \quad (8)$$

Applying the above scaling arguments and equation (8) to the radial momentum balance (2), and assuming that the flow is time independent (i.e., the temporal derivatives are assumed to be zero) it is found that:

1. The convective acceleration terms in the radial momentum balance (equation (3)) are order δ or smaller and can, therefore, be neglected;

2. The centrifugal force is of order unity and is, therefore, non-negligible;

3. The pressure gradient force is of order unity and is, therefore, non-negligible;

4. The Coriolis force is of order unity and is, therefore, non-negligible, and;

5. The summed viscous and Reynolds stresses are of order unity or less, such that some of the terms can be neglected, but others cannot.

Regarding the latter point, *Rozovskii* (1957) details the scaling of the summed viscous and Reynolds stresses. The majority of the Reynolds stresses may be assumed negligible under dimensional analysis, (equation (6)), except for the component of τ_{rz} that is described by $-\upsilon_t \partial u_r/\partial z$, where v_t is the eddy viscosity and the overall term represents the leading order component of turbulence-induced fluid momentum diffusion. Consequently the radial momentum balance (2) simplifies to:

$$\underbrace{\frac{\partial}{\partial z}\nu_t \frac{\partial u_r}{\partial z}}_{\text{turbulent shear stresses}} = \underbrace{\frac{1}{\rho_a}\frac{\partial P}{\partial r}}_{\text{lateral pressure gradient}} - \underbrace{f u_\theta}_{\text{Coriolis acceleration}} - \underbrace{\frac{u_\theta^2}{r}}_{\text{centrifugal acceleration}} \tag{9}$$

where the pressure field is assumed to be hydrostatic and temporal variations (i.e., the inertial terms), convective accelerations and the stress terms (τ_{rr}, τ_{rs}, and a component of τ_{rz}) are neglected. Thus, with these assumptions the leading order behavior of the local radial flow can be understood to be controlled by the balance between the magnitude of the turbulent shear stresses generated by the flow (left-hand side of equation (9)) and the sum of the cross-stream forces, which comprise the lateral pressure gradient, Coriolis force and centrifugal forces, respectively (right-hand side of equation (9)).

1.3. Aims

In this contribution, we present data from a natural field-scale system showing for the first time how velocity and density fields evolve in a natural submarine density current as it flows around a bend. This data is used to resolve the radial momentum balance for the flow as it evolves around the bend. We assess the relative contribution of different terms of the momentum budget (turbulent shear stress, lateral pressure gradient, Coriolis acceleration, and centrifugal acceleration) in controlling bend flow dynamics and we use the residuals of the radial momentum equation to estimate the magnitude of the temporal, convective acceleration, and stress terms neglected in equation (9), henceforth referred to as the nonlocal acceleration term. Our overall aim is to use this novel data set to elucidate the fundamental controls on helical flow within submarine density currents, with implications for both modeling flow dynamics and understanding the sedimentology of submarine sinuous channel systems.

2. Study Area and Methods

2.1. Study Area

Data were collected from a submarine channel system on the Black Sea shelf, immediately to the north of the Strait of Bosphorus in water depths of 70–120 m (Figure 1a). Proximally, the channel system comprises a single trunk channel up to 1.3 km wide and 25 m deep that exhibits a prominent left hand (anticlockwise bend) bend with radius of curvature 3.6 km (using the method of *Richards* [1982]). Distally, the main channel splits into a network of smaller distributary channels. The channel system was initiated ~7.5 ka when a permanent connection was established between the Mediterranean Sea and the Black Sea, via the Strait of Bosphorus. Mediterranean water is ~16–17 psu (practical salinity units) more saline than Black Sea water. This results in an underflow of dense Mediterranean water that passes through the Bosphorus Strait and which, on entering the Black Sea, plunges down to form a stratified gravity current. Interaction of this gravity current with the seafloor has led to the development of the channel system during the past 7.5 ka [*Flood et al*., 2009].

The gravity current has a depth averaged density of 1024 kg/m^3 (based on depth averaging "within channel" density profiles, from the base of the flow to the midpoint of the mixing zone) a maximum thickness of 35 m, and a maximum velocity of ~1.5 m/s. The excess density of the flow (10 kg/m^3) is comparable to values estimated for deep-sea turbidity currents [*Pirmez and Imran*, 2003], albeit in turbidity currents this excess density dominantly results from suspended sediment. Despite being driven by the salinity contrast, the Black Sea gravity current is sufficiently energetic to transport and rework sediment, which is evidenced

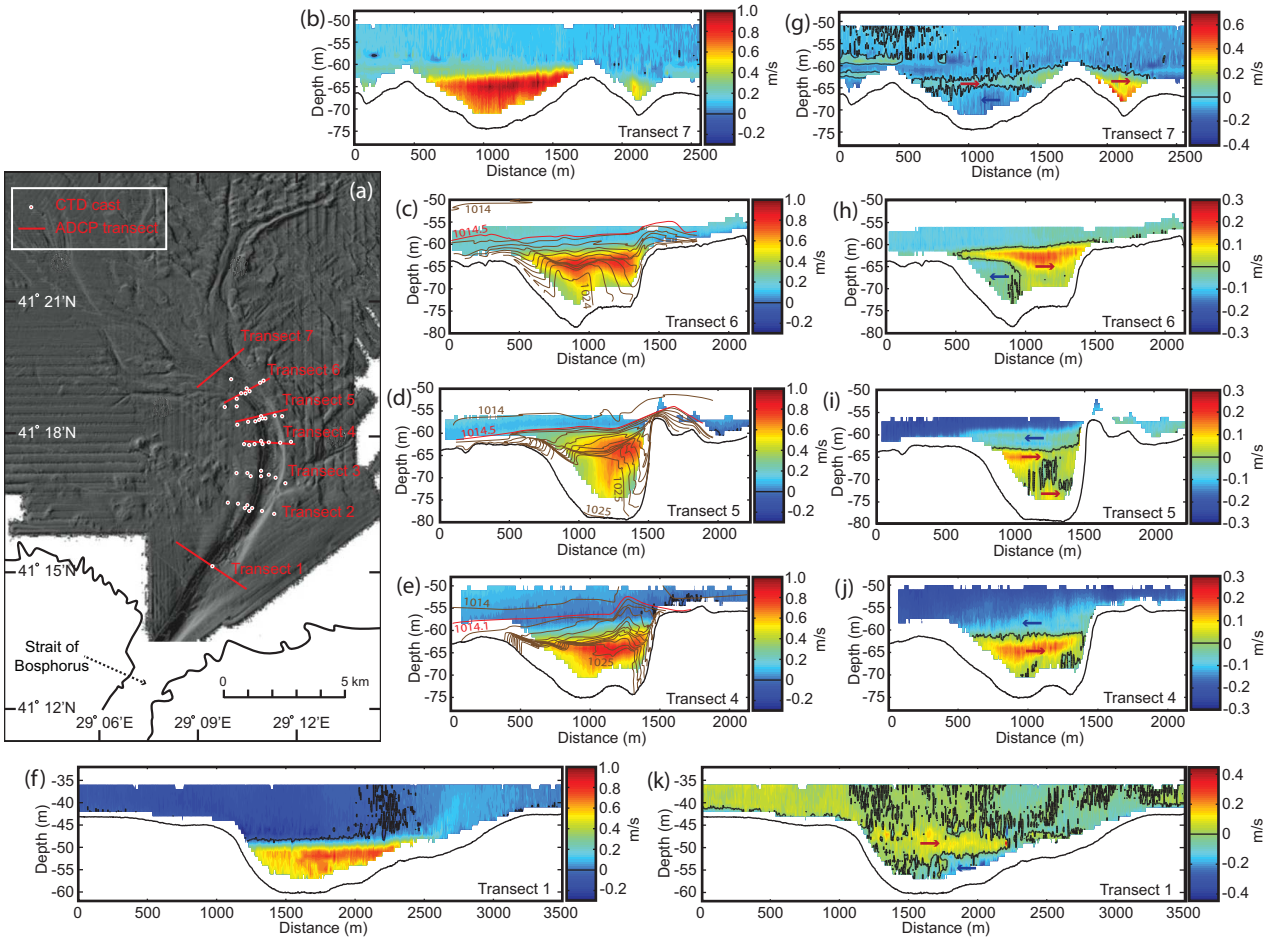

Figure 1. (a) Bathymetric map of the study area showing the locations of all transects and CTD casts used in this study (bathymetry reproduced from *Flood et al.* [2009]). Cross-channel profiles of downstream flow velocities, with density contours superimposed where available (brown lines are contours spaced every 1 kg/m^3, the red contour shows the top of the flow as defined in this study): (b) transect 7; (c) transect 6; (d) transect 5; (e) transect 4; and (f) transect 1. Cross-channel profiles of cross-stream flow velocities. Red and blue arrows highlight regions of positive (toward outer bank) and negative (toward inner bank) flow, respectively: (g) transect 7; (h) transect 6; (i) transect 5; (j) transect 4; and (k) transect 1.

by the presence of large coarse-grained sandy bedforms within the channel network and fine-grained external levees [*Flood et al.*, 2009]. Flow is quasi-continuous, very occasionally being interrupted for short periods when strong onshore winds strengthen Black Sea outflow sufficiently to inhibit inflow of dense Mediterranean water [*Özsoy et al.*, 2001].

Deep-sea turbidity currents have proven notoriously difficult to measure, and thus directly investigate, due to their inaccessible location and infrequent occurrence, which is compounded by present sea-level highstand. The relatively shallow depths of the channel system and the quasi-continuous nature of the Black Sea gravity current flow provide a rare opportunity to study three-dimensional flow dynamics and the interaction of the flow with a seafloor channel network. Thus, it provides a rare analogue for dilute sediment-laden turbidity currents traversing submarine channel systems.

2.2. Methods

The velocity of the gravity current was measured in three components using a 1200 KHz Acoustic Doppler Current Profiler (ADCP), with a vertical bin size of 0.5 m. The ADCP was deployed from *Autosub3*, an autonomous underwater vehicle (AUV), enabling transects of velocity data to be collected. Vertical salinity profiles were measured by deploying a conductivity temperature depth probe (CTD) from a stationary research vessel (RV *Koca Piri Reis*). The ADCP data presented in this study were collected during a 48 h *Autosub3* mission deployed on 22 May 2010 and the CTD data were collected during the period 19–22 May 2010.

Autosub3 was deployed to collect ADCP data along three ~2 km long transects (transects 4–6), perpendicular to the channel axis and spaced roughly equidistantly around the apex of the main channel bend (Figure

1a). Four repeat measurements were made for each of these transects allowing the quantification and identification of coherent flow structures, e.g., helical flow cells [c.f. *Szupiany et al*., 2007; *Parsons et al*., 2013]. In addition, a single ADCP profile was measured for a 3.5 km cross-channel transect close to where the flow exits the mouth of the Bosphorus Strait (transect 1) and a 2 km cross-channel transect distal to the channel bend (transect 7) (Figure 1a). *Szupiany et al*. [2007] demonstrate that single transects are capable of capturing the main flow features, such as helical flow cells, but may lack the finer flow details necessary for quantitative flow analysis. CTD profiles were collected at several points along cross-channel transects (2–6), with an average spacing of ~270 m (Figure 1a). The CTD data were interpolated to the sidewalls by interpolating the data across an adjusted grid [r,z′], where $z' = z - b$ (where z is the original grid and b is the bed depth), and then mapped back onto the real world grid [r,z]. We use a cubic method to interpolate between the data points and to interpolate the data to the channel walls.

The ADCP velocity data were processed using the following steps: (i) position data from the AUV's inertial navigation system were corrected for drift using GPS fixes at the midpoint and end of the AUV survey; (ii) the component of velocity resulting from movement of the AUV was removed from the ADCP-derived flow velocity; (iii) vector data were rotated from a coordinate system relative to the AUV to a global coordinate system; (iv) depth measurements were corrected for vertical offset of the ADCP relative to the AUV's pressure sensor; (v) all data below the maximum ADCP backscatter intensity or within blanking distance (B) of the seafloor were removed, using $B = a\sin^2\alpha$, where a is the altitude of the AUV and α is the angle that the acoustic beam is emitted from the ADCP (20°); (vi) depth data were converted from being relative to the AUV to being relative to the sea surface; (vii) data for individual transects were rotated so that downstream velocities are parallel to the channel walls and cross-stream velocities are perpendicular to this, with positive values denoting outer bank directed flow and negative inner bank directed flow; and (viii) where repeat measurements of a transect were measured, the data were averaged and projected onto a single plane [cf. *Parsons et al*., 2013]. Density was calculated from the salinity and temperature data measured from the CTD using equations presented in *UNESCO* [1983].

2.3. Evaluation of the Radial Momentum Equation

To evaluate the factors forcing the helical flow in the Black Sea density current, herein, we analyze the relative magnitudes of terms in the Reynolds averaged form of the momentum equation (see section 1.2 for derivation):

$$\underbrace{\frac{\partial}{\partial z}\nu_t\frac{\partial u_r}{\partial z}}_{\substack{\text{turbulent}\\ \text{shear}\\ \text{stresses}}} = \underbrace{\frac{1}{\rho_a}\frac{\partial P}{\partial r}}_{\substack{\text{lateral}\\ \text{pressure}\\ \text{gradient}}} - \underbrace{fu_\theta}_{\substack{\text{Coriolis}\\ \text{acceleration}}} - \underbrace{\frac{u_\theta^2}{r}}_{\substack{\text{centrifugal}\\ \text{acceleration}}} \tag{9}$$

The Coriolis parameter was calculated for a latitude (Θ) of 41.3° using $f = 2\Omega\sin\Theta$, where Ω is the Earth's rotation rate. Since, the available field data only describes flow velocity at a point in time and space the Reynolds averaged turbulent motion of flow (i.e., turbulent shear stress) cannot be computed directly [e.g., *Geyer et al*., 2000]. Here, we use the Prandtl mixing length hypothesis to model the turbulent diffusion of fluid momentum (here described as a turbulent shear stress) as the product of an eddy-viscosity and the local gradient of the flow velocity (equation (9)) [*Nielsen and Teakle*, 2004]. Recent work of *Odier et al*. [2009] and *Cossu and Wells* [2012] confirms that, in the shear-layer, the Prandtl mixing-length model well describes the eddy viscosity, as the product of a mixing length and the absolute value of the local flow velocity gradient. *Odier et al*. [2009] propose a scaling for the characteristic mixing length of the flow, in terms of the turbulent energy dissipation rate. However, this argument cannot be replicated or tested here as such field data are not available. Moreover, it is not apparent whether such a model is well suited to describe turbulent mixing at the flow velocity maximum away from the shear-layer of the flow [*Stacey and Bowen*, 1988; *Pope*, 2000]. Alternatively, the eddy viscosity is classically modeled in terms of bulk flow conditions multiplied by some shape factor, detailing vertical variation within the flow. While there exists a range of shape-functions (e.g., constant, linear, parabolic, and piecewise varying, see for example *Dorrell and Hogg* [2012]) to describe the vertical variation of the turbulent mixing within the flow, we employ a parabolic (Rousean) curve, following *Stacey and Bowen* [1988], to describe vertical variation of the eddy-viscosity within the flow.

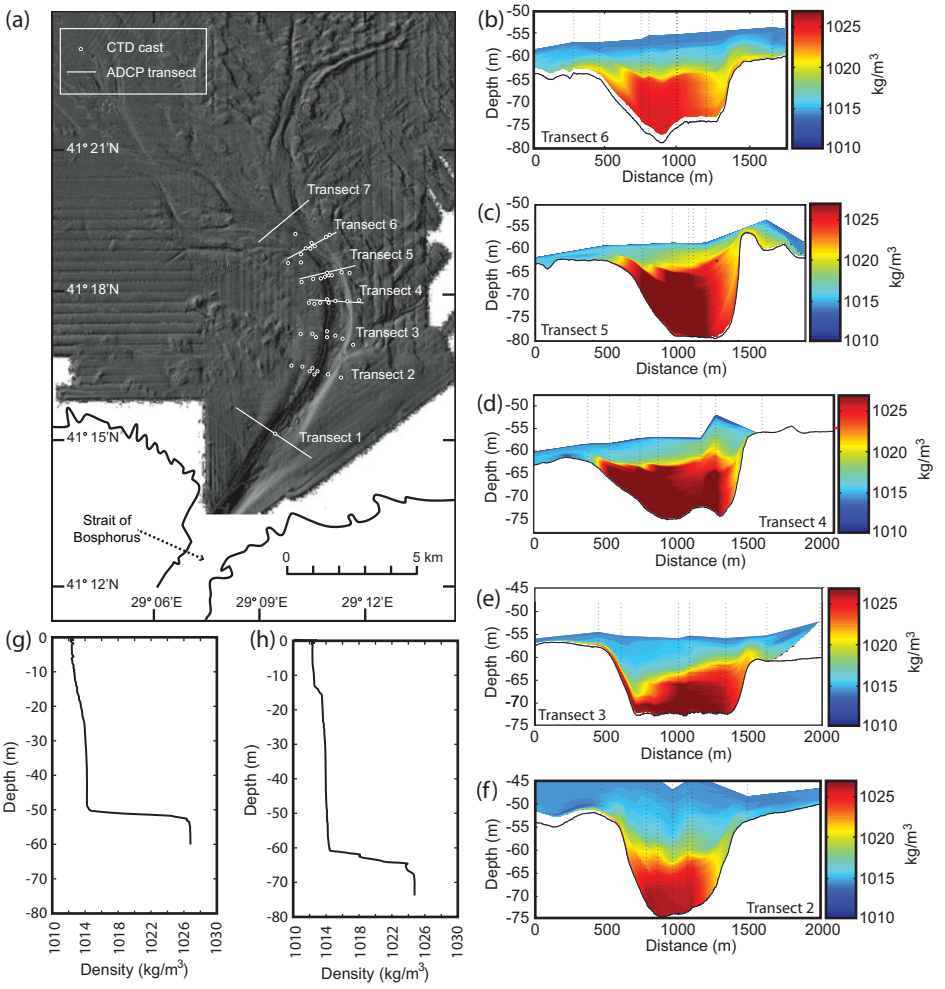

Figure 2. (a) Bathymetric map of the study area showing the locations of all transects and CTD casts used in this study (bathymetry reproduced from *Flood et al.* [2009]). Cross-channel profiles of flow density: (b) transect 6; (c) transect 5; (d) transect 4; (e) transect 3; and (f) transect 2. Density profiles for channel thalweg at (g) transect 1, and (h) ~700 m upstream of transect 7.

In the model, the magnitude of the eddy viscosity is assumed to be proportional to the basal friction velocity, calculated as $\overline{u}_\theta/C_z$ where $\overline{u}_\theta$ is the depth averaged downstream velocity and C_z is the Chezy coefficient. A Chezy coefficient of 8.8 was calculated from flow parameters using the Darcy-Weisbach method [*Soulsby*, 1997]. The pressure gradient term comprises barotropic and baroclinic contributions resulting from flow superelevation and lateral density gradients, respectively. An important consideration in calculating the pressure gradient and shear stress terms is where to define the upper surface of the flow. Previous studies in the Black Sea have defined the ambient fluid density as ~1014 kg/m^3 [e.g., *Latif et al.* 1991]. However, such a value is problematic for the present study. This is most apparent in transect 1 (Figures 1f and 2g), where most material of density 1014–1015 kg/m^3 overlies the gravity current and is moving as a return flow toward the Bosphorus Strait. There is also the consideration, exemplified in transect 6 (Figures 1c and 1h), that much of the material between 1014 and 1015 kg/m^3 is of low downstream velocity (<20 cm/s) and is not involved in the helical flow. We therefore used the downstream and cross-stream velocity data, and the density data in conjunction with one another to define the upper surface of the flow. Thus, the upper surface is defined by a fixed density for each transect but it varies between transects (Figure 1). Having defined the upper surface of the flow the interpolated density data (see section 2.2 for details) were used to compute the pressure gradients in equation (8) and then the integral components, which comprise the transverse water slope (barotropic component) and the radial density gradient and radial structure gradient (baroclinic component).

All the terms in equation (9) are calculable using the data presented in this study. Any discrepancy between the left and right-hand side of equation (9) that is too large to be accounted for through measurement error (see below), is attributable to the combined magnitude of the terms omitted in deriving equation (9), namely (see section 1.2): (i) temporal variations of the flow field (i.e., the inertial terms arising from flow unsteadiness); (ii) the convective acceleration terms from the radial momentum balance (e.g., deviation of the flow from a circular orbit), and (iii) the turbulent stresses neglected from the radial momentum balance. Evaluating the magnitude of the residuals of equation (9) therefore provides a means to evaluate the combined magnitude of these three omitted terms.

The error in each velocity measurement was taken to be a combination of the *error velocity* evaluated by the ADCP and any drift error in the inertial navigation system of the AUV. The *error velocity* is an estimate of the standard deviation in each velocity measurement and is evaluated from the difference in calculations of velocity using different combinations of three of the four ADCP beams [*Oberg and Mueller*, 2007]. These error velocities were propagated through the equations used to calculate centrifugal acceleration, Coriolis acceleration, and turbulence shear stress, and the resulting uncertainties were found to be of the order $O(10^{-8})$, $O(10^{-7})$, and $O(10^{-7})$, respectively. The manufacturer's resolution estimates for salinity (0.4 ppm) and temperature (0.0001°C) were used to estimate the error in the density measurement by propagating them through the equations presented in *UNESCO* [1983], resulting in uncertainty in the density measurements of ± 0.08 kg/m^3. The difference between the resulting lateral pressure gradients calculated with positive and negative density error was taken as an estimate of the uncertainty in the lateral pressure gradients and was found to be $O(10^{-5})$. The error in the lateral momentum term $O(10^{-5})$ was the maximum value found by combining the errors in the lateral pressure gradients, centrifugal, and Coriolis forces. In all cases, these terms were found to be at least two orders of magnitude larger than their respective errors.

3. Results

3.1. Velocity and Density Magnitude and Distribution

On exiting the Strait of Bosphorus the gravity current comprises a high-density core ~10 m thick, which is confined within the channel. Overlying this there is an unconfined dilute flow phase ~30 m thick that is travelling slowly (<0.2 m/s) in the opposite direction to the gravity current; this is the return part of the exchange flow between the Marmara Sea and the Black Sea via the strait of Bosphorus. Maximum velocity (0.9 m/s) is located 7 m ($z/H = 0.7$) above the seafloor, although there is no distinct velocity core (Figure 1f). Cross-channel velocities reveal a single helical circulation cell, with a clockwise (river-like) orientation when viewed looking downstream (Figure 1k). Downstream of transect 1, and before transect 2, there is a region containing hydraulic jumps [*Sumner et al.,* 2013]. Density transects in the region prior to the bend apex (transects 2 and 3) reveal that the density core of the flow is located low down and centrally (Figures 2e and 2f) and that the flow is up to ~20 m thick and is not fully confined within the channel.

Prior to the bend apex (transect 4) the gravity current is up to ~20 m thick at the outer bend where the flow is superelevated (Figure 1e) but does not appear to overspill significantly at the time of survey (Figures 1e and 2d). Flow is unconfined at the inside bend. The densest part of the flow is spread across the channel width (Figures 1e and 2d). The velocity maximum (0.89 m/s) is located centrally within the channel, and at an elevation of 10 m ($z/H = 0.5$) above the channel floor. Cross-channel flow is dominated by a counter-clockwise helical circulation cell, with flow directed toward the outer bank at the base of the flow, and toward the inner bank at the top of the flow. There is some weak inwardly directed flow, toward the bottom of the flow, at the outer bank (Figure 1j). The channel is 1283 m wide and 19 m deep, the positive relief in the base of the channel is a bar form dominantly comprising coarse-grained sand.

Downstream of the bend apex (transect 5) the gravity current is up to ~ 20 m thick and flow is unconfined on both sides of the channel (Figures 1d, 1i, and 2c), with the flow superelevated toward the outside of the bend. The density core is located toward the inside bend, whereas the velocity maximum (0.81 m/s) is located toward the outer bend at an elevation of 15 m ($z/H = 0.75$) above the channel floor (Figures 1d and 2c). Cross-channel flow is complex, with the lower half of the flow being dominantly outward directed but with some low velocity inwardly directed flow within this zone. Helical flow toward the flow top is inwardly directed (Figure 1i). The channel at this location is deeper (22 m) and narrower (882 m) than upstream with a prominent aggradational levee on the outer bank.

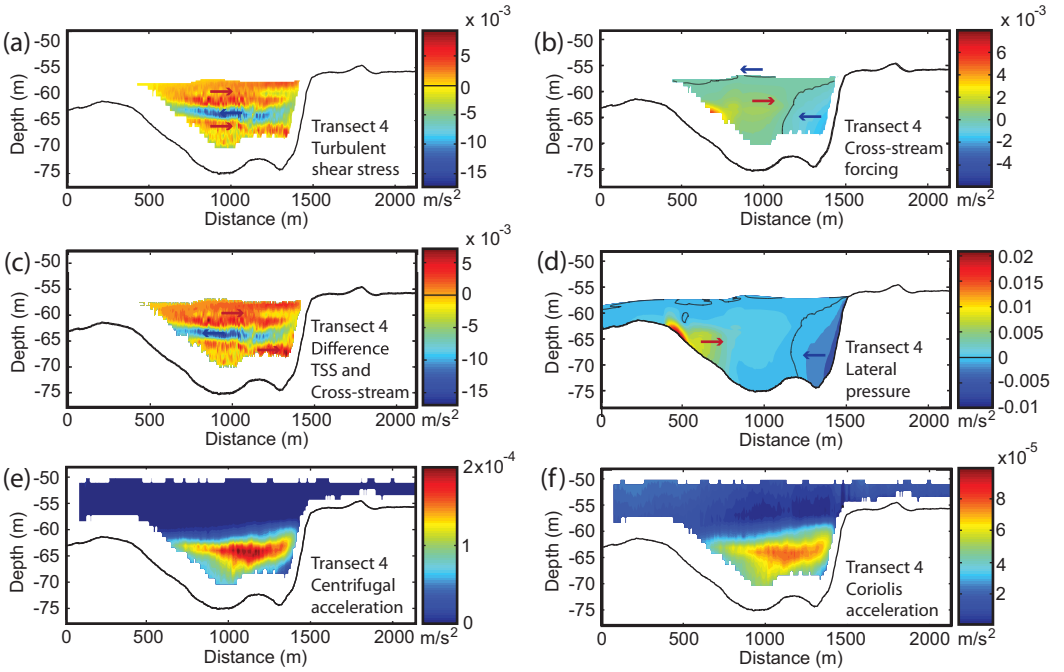

Figure 3. Transect 4: (a) turbulent shear stress; (b) cross-stream forcing; (c) difference between turbulent shear stress and cross-stream forcing; (d) lateral pressure gradient; (e) centrifugal acceleration; and (f) Coriolis acceleration. Red and blue arrows highlight regions with positive (toward outer bank) and negative (toward inner bank) acting forces, respectively.

On exiting the bend (transect 6), the flow is up to ~20 m thick and flow is unconfined by the channel (Figures 1c, 1h, and 2b). The density core has returned to being centrally located and the flow remains slightly superelevated at the outer bend (Figure 2b). The flow displays a double downstream velocity core, with a maximum velocity of 0.84 m/s located centrally within the left hand velocity core, at an elevation of 14 m ($z/H = 0.7$) above the channel floor. Helical flow is complex displaying both weak inward and weak outward directed flow at the flow base, strongly outwardly directed flow toward the top of the channel, and inwardly directed flow at the flow top (Figure 1h). The channel has returned to being shallower (18 m) and wider (1066 m), with a bar form comprising coarse sand at the outer channel wall.

Distal to the bend (transect 7), the flow is ~ 15 m thick (Figures 1b, 1g, and 2h). The density profile in Figure 2h was taken 700 m upstream of transect 7 and shows that the flow has a dense component ~8 m thick overlain by a more dilute flow phase. At the location of the transect, the velocity core is located some 9 m ($z/H = 0.6$) above the channel floor and has a maximum velocity of 1.04 m/s. Helical flow in the main channel manifests as a clockwise directed helical circulation (looking downstream) with inward directed basal flow, and flow that overspills into a smaller channel to the east (Figure 2e).

It is not possible to image the near-bed region of the flow using an ADCP because of acoustic side-lobe interference. Therefore, we cannot be certain about the nature of the cross-stream flow in a zone close to the bed region. However, the available data and previous data do suggest that near-bed flow is outwardly directed at the bend apex. First, our measurements closest to the bed in transect 5 at the bend apex are all outwardly directed. Second, previous data from the bend axis where the flow was imaged closer to the bed is also outwardly directed [*Parsons et al*, 2010].

3.2. Evaluation of Terms of the Lateral Momentum Equation

The terms of the radial momentum equation (9) were evaluated for the three transects (transects 4–6) for which both velocity and density data were collected (Figures 3–5). Recall that the left-hand side of this equation (9) represents the shear stress generated by the flow ($O(10^{-2}-10^{-3})$), and the right-hand side represents the cross-stream forces acting on the flow ($O(10^{-3})$) which comprises the pressure gradient, centrifugal force, and Coriolis force. The data reveal that for all of the transects the shear stress and cross-stream forcing are of similar orders of magnitude, however, their structures can be very different (Figures 3–5). The

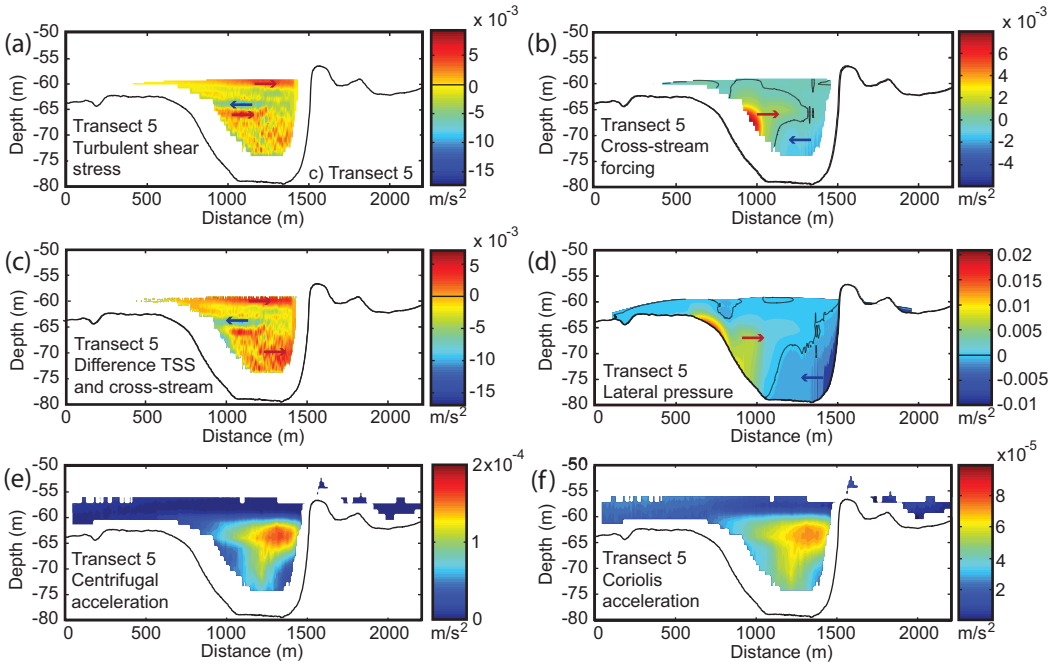

Figure 4. Transect 5: (a) turbulent shear stress; (b) cross-stream forcing; (c) difference between turbulent shear stress and cross-stream forcing; (d) lateral pressure gradient; (e) centrifugal acceleration; and (f) Coriolis acceleration. Red and blue arrows highlight regions with positive (toward outer bank) and negative (toward inner bank) acting forces, respectively.

cross-stream forcing ($O(10^{-3})$) is always dominated by the pressure term ($O(10^{-2}-10^{-3})$), with minor contributions from the centrifugal acceleration ($O(10^{-4})$) and the Coriolis force ($O(10^{-5})$).

The distribution of shear stress shown in Figures 3–5 is complex and varies for the different transects, particularly in the vertical position of inwardly directed shear stress. All three transects exhibit similar structures

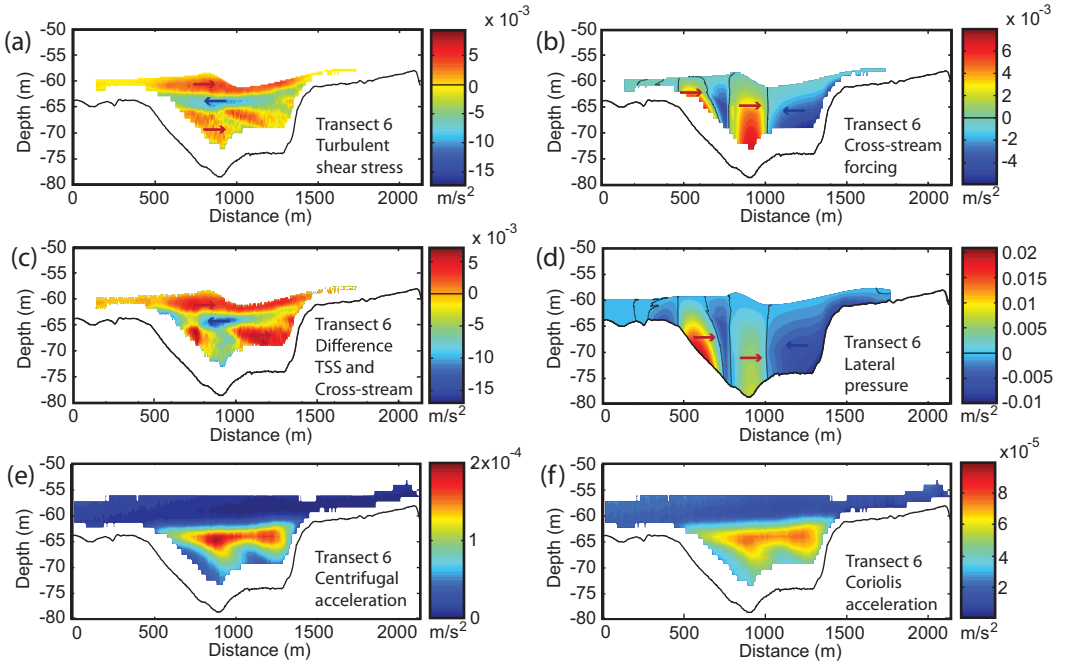

Figure 5. Transect 6: (a) turbulent shear stress; (b) cross-stream forcing; (c) difference between turbulent shear stress and cross-stream forcing; (d) lateral pressure gradient; (e) centrifugal acceleration; and (f) Coriolis acceleration. Red and blue arrows highlight regions with positive (toward outer bank) and negative (toward inner bank) acting forces, respectively.

for pressure gradients, centrifugal forces, and Coriolis forces. Pressure gradients are dominantly outwardly directed at the inside bend and inwardly directed at the outer bend, with the highest pressure gradients located toward the base of the flow. In all three transects (4–6), the highest pressure gradients are outwardly directed. The centrifugal forces and Coriolis forces are always outwardly directed throughout the flow depth with their maxima corresponding to the height of the velocity maxima.

3.3. Evaluation of Nonlocal Accelerations

If the flow were well described by the radial momentum balance presented in equation (9), then we would expect the turbulence shear stress generated by the flow and the cross-stream forces acting on the flow to be approximately balanced (Figures 3–5). While the turbulent shear stress and cross stream forcing are of similar magnitude (both $O(10^{-3})$), their structures vary significantly and this results in the difference between the two terms also being of $O(10^{-3})$. This discrepancy is too large to be attributed to measurement error (see section 2.4). It is most likely that the forces do not balance because of nonlocal accelerations of the flow due to additional forces such as topographic forcing due to changes in channel shape [e.g., *Dietrich and Smith*, 1983; *Nelson and Smith*, 1989] and downstream advection of the flow [e.g., *Furbish*, 1987]. Importantly, this nonlocal acceleration term is of similar order of importance in the cross-stream force balance as the lateral pressure gradient and is of greater magnitude than either the centrifugal or Coriolis forces acting on the flow.

4. Discussion

In the following section, we consider why the velocity and density maxima decouple as the flow goes around the bend. We then discuss the implications of this decoupling for understanding the fundamental controls on the orientation of helical flow in submarine gravity currents. Finally, we highlight factors that must be considered in future numerical models in order for them to accurately represent their natural counterparts.

4.1. Why Do Velocity and Density Decouple Around the Bend?

As the flow travels around the bend, the velocity maximum and the density maximum decouple. The velocity maximum moves upward and outward, whereas the density maximum hugs the inner channel bend (Figures 1 and 2). This decoupling is important because this density distribution strongly influences the cross-stream pressure gradient, which is the leading order term in the cross-stream force balance. Decoupling of velocity and density, with the density maximum hugging the inside channel bend is not unique to this study but has also been observed in field studies of stratified flows in curved estuaries [*Seim and Gregg*, 1997; *Nidzieko et al*., 2009] and a stratified gravity current travelling through a curved channel-like constriction in the western Baltic Sea [*Umlauf et al*., 2007; *Umlauf and Arneborg*, 2009a, 2009b]. In all of these cases, this density distribution is associated with nonriver-like helical flow structures, i.e., flow reversal and/or multiple stacked flow cells.

To understand the cross-channel force balance and the structure of helical flow cells, it is important to consider why density and velocity decouple and how the density maximum ends up at the inside bend. *Seim and Gregg* [1997] suggest that river-like helical flow prior to the channel bend forces the dense fluid to the inner channel wall, it then causes the dense fluid to be lifted up and for the flow to overturn and mix. We infer a similar process for the Black Sea (Figure 6). Inwardly directed near-bed flow prior to the bend pushes the density maximum inward. However, due to the higher density and greater stratification in the Black Sea, the flow has insufficient energy to lift the dense fluid and instead it remains trapped at the inner bend whereby it sets up a pressure gradient into the interior of the flow which contributes significantly to flow reversal (Figure 6).

Two previous numerical modeling studies have considered the detailed cross-channel density distribution of a channelized submarine gravity current travelling around a bend [*Giorgio Serchi et al*., 2011; *Janocko et al*., 2013]. These two models display different results. Contrary to our data, *Giorgio Serchi et al*. [2011] show that at the channel apices the density maximum is shifted toward the outer bend. It is only as the flow is entering the second bend that the density maximum is located toward the inside bend. However, this density distribution is rapidly obliterated because of strong centrifugal forces. In contrast, the model of *Janocko et al*. [2013] shows similarities with our results, with the density maximum located at the inner

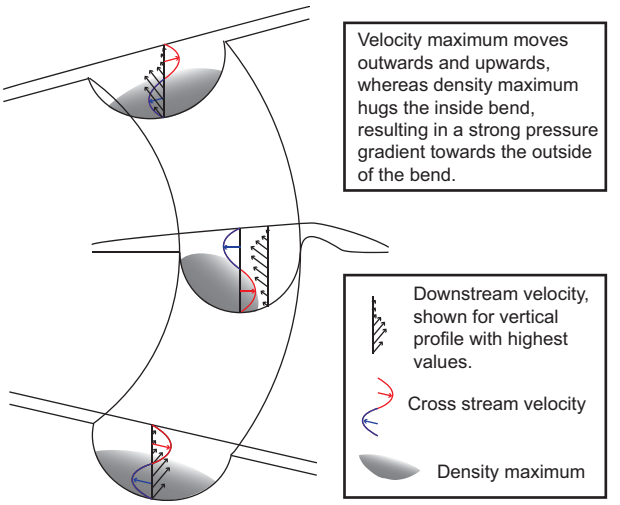

Figure 6. Schematic diagram showing decoupling of velocity and density maxima. The location of the density maxima at the inside channel bend results in a strong cross-channel pressure gradient toward the outer channel bend.

channel bend up until the bend apex. This apparent contradiction between the models may be explained by the relative magnitudes of the centrifugal acceleration and radial pressure gradients acting on the different flows. The numerical models of *Giorgio Serchi et al.* [2011] and *Janocko et al.* [2013] both have tight bends ($R/w = 2.3$ and 1.5, respectively: R is radius of curvature and w is channel width) relative to the Black Sea bend ($R/w = 3.3$). The velocities of the bend flows in *Giorgio Serchi et al.* [2011] and *Janocko et al.* [2013] are 0.6 and 0.16 m/s, respectively. However, the excess densities used in the two numerical models are very different: *Giorgio Serchi et al.* [2011] used an excess density of 3.3%, whereas *Janocko et al.* [2013] used excess densities between 13.25% and 39.75%. Thus, it seems likely that the very large excess densities used in *Janocko et al.* [2013] result in radial pressure gradients that dominate over centrifugal forces as the flow travels around the bend. Thus, these studies support the assertion that centrifugal forces are likely to dominate in studies with weakly stratified flows and tight bends, whereas radial pressure gradients will dominate for stratified flows travelling around more open bends. Therefore, decoupling of the velocity and density maxima is most likely to predominate for stratified flows travelling around relatively open bends.

4.2. What are the Fundamental Controls on Helical Flow in Submarine Density Currents?

As the Black Sea density current flows around the bend the velocity core moves outward and upward and there is superelevation of flow at the outer bend. As discussed above, the dense core of the flow hugs the inner bend (Figure 6). This results in lateral pressure gradients directed toward the interior of the flow that result from flow superelevation at the outer bend and pressure gradients resulting from the density core at the inner bend. Centrifugal acceleration and Coriolis acceleration provide more minor contributions to the outwardly directed flow, with their maxima corresponding to the vertical location of the downstream velocity maxima.

We find that there is a significant imbalance in our closure of the lateral momentum budget as expressed by equation (9), meaning that an important term or terms (nonlocal acceleration) are missing from that balance. This missing term, or terms, is of similar magnitude to the contribution from the lateral pressure gradients. This nonlocal acceleration term likely includes contributions from topographic steering due to changes in gross channel shape and internal architecture such as large-scale bed and bar forms [*Dietrich and Smith*, 1983; *Legleiter et al.*, 2011]. This likely explains some of the complexity observed in the helical flow structure around the bend apex, where the channel changes shape and there are prominent barforms toward the outer channel wall. Downstream advection of the flow means that there is a lag time between the forces acting on the flow and the development or adjustment of helical flow [*Furbish*, 1987; *Chant and Wilson*, 1997], this makes it inappropriate to balance cross-stream flow in any two-dimensional cross section.

The key result from this study is that whereas previous work has assumed that centrifugal forces are the primary control on the orientation of helical flow cells, we find that in the Black Sea gravity flow, lateral pressure gradients, and nonlocal acceleration of the flow are the leading order terms in the lateral momentum budget. We acknowledge that the force balance acting on other systems may differ. In particular, centrifugal forces may dominate lateral pressure gradients in systems with tighter bends and faster flows; moreover, sediment-laden flows may adjust their stratification differently to the saline flow studied here. However, this

study shows strong agreement with complementary studies of stratified flows in curved estuaries where it has been shown that, in weakly stratified flows, the centrifugal forces dominate the lateral momentum budget, whereas in highly stratified flows lateral pressure gradients can dominate instead [*Lacy and Monismith*, 2001; *Nidzieko et al*., 2009]. In estuaries, river-reversed helical circulation is the exception rather than the norm because well-mixed flows are more common than stratified flows. However, in submarine channels river-reversed helical flow cells and complex helical flow structures may be more common as highly stratified flows are likely to be common, particularly in proximal settings [*Stacey and Bowen*, 1988; *Hiscott et al*., 1997; *Peakall et al*., 2000].

4.3. Implications for Modeling Curvature-Induced Lateral Circulation in Submarine Flows

This study highlights that lateral pressure gradients and nonlocal accelerations can be leading order terms in the cross-stream force balance. This has several implications for accurately modeling flows. First, cross-channel density gradients cannot be ignored. Second, three-dimensional models are required to accurately predict cross-stream flow patterns. Third, changes in channel shape and topography may be of equal importance in controlling the structure of helical flow cells as either centrifugal forces or lateral pressure gradients.

With the exception of *Giorgio Serchi et al*. [2011] and *Janocko et al*. [2013], previous models of flow in submarine channels have not considered lateral density gradients. In this study (Black Sea), and others [e.g., *Seim and Gregg*, 2009; *Nidzieko et al*., 2009], strong lateral density gradients result in lateral pressure gradients that are the dominant term in the cross-stream force balance. The nonlocal acceleration term includes contributions from topographic forcing and downstream advection of the circulation cell that results in a spatial and temporal lag in the flow reacting to the forces acting upon it. Without further detailed measurements, we cannot evaluate the magnitudes of the different contributions to the nonlocal acceleration term. It is clear that the shape of the channel varies significantly around the bend, and that this is likely to impact on helical flow structure [*Dietrich and Smith*, 1983; *Legleiter et al*., 2011]. This suggests a potential source of error in models with a fixed channel geometry. The spatial and temporal lag in the flow reacting to the forces acting upon it seriously questions the ability of two-dimensional models to accurately capture cross-stream flow dynamics.

5. Conclusions

We present an exceptional data set that illustrates how the three-dimensional velocity and density of a submarine gravity current evolves as it travels through a sinuous channel system on the Black Sea shelf. This gravity current provides a rare analogue to turbidity currents in the deep sea, for which there are few direct measurements [*Talling et al*., 2012]. Helical or cross-channel flow is a major control on the morphodynamics of channel systems [*Darby and Peakall*, 2012]. Prior to the channel bend, the Black Sea flow exhibits river-like helical flow, with near-bed fluid directed toward the inner bend. As the flow travels around the bend, the direction of near-bed flow reverses and complex helical flow patterns are observed. Following the bend, the near-bed helical flow returns to being directed toward the inner bend. Existing models tend to assume that the orientation of helical flow in submarine gravity currents is controlled by centrifugal- and Coriolis-induced accelerations. In contrast, calculation of the forces acting on the Black Sea gravity current reveal that lateral pressure gradients resulting from flow stratification are the dominant force in the cross-stream momentum balance. This results, in part, from decoupling of the velocity and density maxima as the flow goes around the bend, with the high density fluid at the inside bend causing strong pressure gradients directed toward the interior of the flow. By analogy with estuarine flows, the domination of radial pressure gradients over centrifugal forces is likely to occur in highly stratified flows traveling around relatively open bends as is likely to be the case for many naturally occurring turbidity currents. Our analysis also demonstrates that nonlocal acceleration terms, which may be due to topographic forcing and downstream advection of cross-stream flow, are important terms in the cross-stream momentum balance. The major implications of this work for conceptual and numerical modeling are that three-dimensional models that incorporate lateral flow stratification are required to accurately model curvature-induced helical flow, and that changes in channel geometry may contribute significantly to the forces acting on the flow.

Acknowledgments
This project was funded by Natural Environment Research Council grants NE/F020511/1, NE/F020120/1, and NE/F020279/1. We thank Rick Hiscott and Ali Aksu of Memorial University, Canada, Roger Flood of Stony Brook University, USA, and Dogan Yasar of Dokuz Eylül University, Turkey, along with the Master and crew of the RV *Koca Piri Reis* for their assistance with cruise planning and operation.

References

Abad, J. D., O. E. Sequeiros, B. Spinewine, C. Pirmez, M. H. Garcia, and G. Parker (2011), Secondary current of saline underflow in a highly meandering channel: Experiments and theory, *J. Sediment. Res.*, *81*, 787–813, doi:10.2110/jsr.2011.61.

Amos, K. J., J. Peakall, P. W. Bradbury, M. Roberts, G. Keevil, and S. Gupta (2010), The influence of bend amplitude and planform morphology on flow and sedimentation in submarine channels, *Mar. Petrol. Geol.*, *27*, 1431–1447, doi:10.1016/j.marpetgeo.2010.05.004.

Babonneau, N., B. Savoye, M. Cremer, and M. Bez (2010) Sedimentary architecture in meanders of a submarine channel: Detailed study of the present Congo turbidite channel (Zaiango project), *J. Sediment. Res.*, *80*, 852–866, doi:10.2110/jsr.2010.078.

Chant, R. J., and R. E. Wilson (1997), Secondary circulation in a highly stratified estuary, *J. Geophys. Res.*, *102*(C10), 23,207–23,215.

Cheng, P., R. E. Wilson, R. J. Chant, D. C. Fugate, and R. D. Flood (2009), Modeling influence of stratification on lateral circulation in a stratified estuary, *J. Phys. Oceanogr.*, *39*, 2324–2337, doi:10.1175/2009JPO4157.1.

Corney, R. K. T., J. Peakall, D. R. Parsons, L. Elliott, K. J. Amos, J. L. Best, G. M. Keevil, and D. B. Ingham (2006), The orientation of helical flow in curved channels, *Sedimentology*, *53*, 249–257.

Corney, R. K. T., J. Peakall, D. R. Parsons, L. Elliott, K. J. Amos, J. L. Best, G. M. Keevil, and D. B. Ingham (2008), Reply to discussion of Imran et al. on "The orientation of helical flow in curved channels," *Sedimentology*, *55*, 241–247, doi:10.1111/j.1365–3091.2006.00771.x.

Cossu, R., and M. G. Wells (2010), Coriolis forces influence the secondary circulation of gravity currents flowing in large-scale sinuous submarine channel systems, *Geophys. Res. Lett.*, *37*, L17603, doi:10.1029/2010GL044296.

Cossu, R., and M. G. Wells (2012) A comparison of the shear stress distribution in the bottom boundary layer of experimental density and turbidity currents, *Eur. J. Mech. B*, *32*, 70–79, doi:10.1016/j.euromechflu.2011.09.006.

Cossu, R., and M. G. Wells (2013), The evolution of submarine channels under the influence of Coriolis forces: Experimental observations of flow structures, *Terra Nova*, *25*, 65–71, doi:10.1111/ter.12006.

Darby, S. E., and J. Peakall (2012), Modelling the equilibrium bed topography of submarine meanders that exhibit reversed secondary flows, *Geomorphology*, *163–164*, 99–109, doi:10.1016/j.geomorph.2011.04.050.

Dietrich, W. E., and J. D. Smith (1983), Influence of the point-bar on flow through curved channels, *Water Resour. Res.*, *19*, 1173–1192.

Dorrell, R., and A. Hogg (2012), Length and time scales of response of sediment suspensions to changing flow conditions, *J. Hydraul. Eng.*, *138*, 430–439, doi:10.1061/(ASCE)HY.1943–7900.0000532.

Dorrell, R. M., S. E. Darby, J. Peakall, E. J. Sumner, D. R. Parsons, and R. B. Wynn (2013), Superelevation and overspill control secondary flow dynamics in submarine channels, *J. Geophys. Res.*, *118*, 3895–3915, doi:10.1002/jgrc.20277.

Emmel, F. J., and J. R. Curray (1983), The Bengal submarine fan, Northeastern Indian Ocean, *Geo Mar. Lett.*, *3*, 119–124.

Felix, M. (2002), Flow structure of turbidity currents, *Sedimentology*, *49*, 397–419.

Fer, I., G. Voet, K. S. Seim, B. Rudels, and K. Latarius (2010), Intense mixing of the Faroe Bank Channel overflow, *Geophys. Res. Lett.*, *37*, L02604, doi:10.1029/2009GL041924.

Flood, R. D., R. N. Hiscott, and A. E. Aksu (2009), Morphology and evolution of an anastomosed channel network where saline underflow enters the Black Sea, *Sedimentology*, *56*, 807–839, doi:10.1111/j.1365–3091.2008.00998.x.

Furbish, D. J. (1987), Conditions for geometric similarity of coarse stream-bed roughness, *Math. Geol.*, *4*, 291–307.

Garcia, M. H., and G. Parker (1989), Experiments on hydraulic jumps in turbidity currents near a canyon-fan transition, *Science*, *245*, 393–396.

Geyer, W. R. (1993), Three-dimensional tidal flow around headlands, *J. Geophys. Res.*, *98*, 955–966.

Geyer, W. R., J. H. Trowbridge, and M. M. Bowen (2000), The dynamics of a partially mixed estuary, *J. Phys. Oceanogr.*, *30*, 2035–2048.

Giorgio Serchi, F., J. Peakall, D. B. Ingham, and A. D. Burns (2011), A unifying computational fluid dynamics investigation of the river-like to river-reversed secondary circulation in submarine channel bends, *J. Geophys. Res.*, *116*, C06012, doi:10.1029/2010C006361.

Hiscott, R. N., F. R. Hall, and C. Pirmez (1997), Turbidity-current overspill from the Amazon channel: Texture of the silt/sand load, paleoflow from anisotropy of magnetic susceptibility and implications for flow processes, in *Proc. Ocean Drill. Prog. Sci. Results*, vol. *155*, edited by R. D. Flood et al., pp. 53–78, Ocean Drilling Program, College Station, Tex.

Huang, H., J. Imran, and C. Pirmez (2012), The depositional characteristics of turbidity currents in submarine sinuous channels, *Mar. Geol.*, *329*, 93–102, doi:10.1016/j.margeo.2012.08.003.

Imran, J., G. Parker, and C. Pirmez (1999), A nonlinear model of flow in meandering submarine and subaerial channels, *J. Fluid Mech.*, *400*, 295–331.

Imran, J., M. A. Islam, H. Q. Huang, A. Kassem, J. Dickerson, C. Pirmez, and G. Parker (2007), Helical flow couplets in submarine gravity underflows, *Geology*, *35*, 659–662, doi:10.1130/G23780A.1.

Islam, M. A., and J. Imran (2008), Experimental modelling of gravity underflow in a sinuous submerged channel, *J. Geophys. Res*, *113*, C07041, doi:10.1029/2007JC004292.

Janocko, M., M. B. J. Cartigny, W. Nemec, and E. W. M. Hansen (2013), Turbidity current hydraulics and sediment deposition in erodible sinuous channels: Laboratory experiments and numerical simulations, *Mar. Petrol. Geol.*, *41*, 222–249, doi:10.1016/j.marpetgeo.2012.08.012.

Kassem, A., and J. Imran (2004), Three dimensional modeling of a density current: II: Flow in sinuous confined and unconfined channels, *J. Hydraul. Res.*, *42*, 591–602.

Keevil, G. M., J. Peakall, J. L. Best, and K. J. Amos (2006), Flow structure in sinuous submarine channels: Velocity and turbulence structure of an experimental submarine channel, *Mar. Geol.*, *229*, 241–257, doi:10.1016/j.margeo.2006.03.010.

Keevil, G. M., J. Peakall, and J. L. Best (2007), The influence of scale, slope and channel geometry on the flow dynamics of submarine channels, *Mar. Petrol. Geol.*, *24*, 487–503, doi:10.1016/j.marpetgeo.2007.01.009.

Khripounoff, A., A. Vangriesheim, N. Babonneau, P. Crassous, B. Dennielou, and B. Savoye (2003), Direct observation of intense turbidity current activity in the Zaire submarine valley at 4000 m water depth, *Mar. Geol.*, *194*, 151–158, doi:10.1016/S0025–3227(02)00677-1.

Klaucke, I., and R. Hesse (1996), Fluvial features in the deep-sea: New insights from the glacigenic submarine drainage system of the Northwest Atlantic Mid-Ocean Channel in the Labrador Sea, *Sediment. Geol.*, *106*, 223–234.

Kolla, V., H. W. Posamentier, and L. J. Wood (2007), Deep-water and fluvial sinuous channels: Characteristics, similarities and dissimilarities, and modes of formation, *Mar. Petrol. Geol.*, *24*, 388–405, doi:10.1016/j.marpetgeo.2007.01.007.

Komar, P. D. (1969), The channelized flow of turbidity currents with application to Monterey deep-sea fan channel, *J. Geophys. Res.*, *74*, 4544–4558.

Lacy, J. R., and S. G. Monismith (2001), Secondary currents in a curved, stratified, estuarine channel, *J. Geophys. Res.*, *106*, 31,283–31,302.

Latif, M. A., E. Özsoy, T. Oguz, and Ü. Ünlüata (1991), Observations of the Mediterranean inflow into the Black Sea, *Deep Sea Res. Part A*, *38*, S711–S723.

Legleiter, C. J., L. R. Harrison, and T. Dunne (2011), Effect of point bar development on the local force balance governing flow in a simple, meandering gravel bed river, *J. Geophys. Res.*, *116*, F01005, doi:10.1029/2010JF001838.

Mahdinia, M., B. Firoozabadi, M. Farshchi, A. G. Varnamkhasti, and H. Afshin (2012), Large eddy simulation of lock-exchange flow in a curved channel, *J. Hydraul. Eng.*, *138*, 57–70, doi:10.1061/(ASCE)HY.1943–7900.0000482.
Manica, R. (2012), Sediment gravity flows: Study based on experimental simulations, in *Hydrodynamics: Natural Water Bodies*, edited by H. E. Schulz, A. L. A. Simões, and R. J. Lobosco, pp. 263–286, InTech, Rijeka, Croatia.
Mayall, M., E. Jones, and M. Casey (2006), Turbidite channel reservoirs: Key elements in facies prediction and effective development, *Mar. Petrol. Geol.*, *23*, 821–841, doi:10.1016/j.marpetgeo.2006.08.001.
Meiburg, E., and B. Kneller (2010), Turbidity currents and their deposits, *Annu. Rev. Fluid Mech.*, *42*, 135–156, doi:10.1146/annurev-fluid-121108–145618.
Nelson, J. M. and J. D. Smith (1989), Evolution and stability of erodible channel bends, in *River Meandering*, edited by S. Ikeda and G. Parker, pp. 948–970, AGU, Washington, D. C.
Nidzieko, N. J., J. L. Hench, and S. G. Monismith (2009), Lateral circulation in well-mixed and stratified estuarine flows with curvature, *J. Phys. Oceanogr.*, *39*, 831–851, doi:10.1175/2008JPO4017.1.
Nielsen, P., and I. A. L. Teakle (2004), Turbulent diffusion of momentum and suspended particles: A finite-mixing-length theory, *Phys. Fluids*, *16*, 2342–2348, doi:10.1063/1.1738413.
Oberg, K. A., and D. S. Mueller (2007), Validation of streamflow measurements made with acoustic current profilers, *J. Hydraul. Eng.*, *33*, 1422–1432, doi:10.1061/(ASCE)0733–9429(2007)133:12(1421).
Odier, P., J. Chen, M. K. Rivera, and R. E. Ecke (2009), Fluid mixing in stratified gravity currents: The Prandtl mixing length, *Phys. Rev. Lett.*, *102*, 134,504, doi:10.1103/PhysRevLett.102.134504.
Özsoy, E., D. Di Iorio, M. C. Gregg, and J. O. Backhaus (2001), Mixing in the Bosphorous Strait and the Black Sea continental shelf: Observations and a model of the dense water outflow, *J. Mar. Syst.*, *31*, 99–135.
Parsons, D. R., J. Peakall, A. E. Aksu, R. D. Flood, R. N. Hiscott, S. Besiktepe, and D. Mouland (2010), Gravity-driven flow in a submarine channel bend: Direct field evidence of reversed helical flow reversal, *Geology*, *38*, 1063–1066, doi:10.1130/G31121.1.
Parsons, D. R., P. R. Jackson, J. A. Czuba, F. L. Engel, B. L. Rhoads, K. A. Oberg, J. L. Best, D. S. Mueller, K. K. Johnson, and J. D. Riley (2013) Velocity Mapping Toolbox (VMT): A processing and visualization suite for moving-vessel ADCP measurements, *Earth Surf. Processes Landforms*, *38*, 1244–1260, doi:10.1002/esp.3367.
Paull, C. K., W. Ussler III, H. G. Greene, R. Keaten, P. Mitts, and J. Barry (2003), Caught in the act: The 20 December 2001 gravity flow event in Monterey Canyon, *Geo Mar. Lett.*, *22*, 227–232, doi:10.1007/s00367–00300117-2.
Peakall, J., B. McCaffrey, and B. Kneller (2000), A process model for the evolution, morphology, and architecture of sinuous submarine channels, *J. Sediment. Res.*, *70*, 434–448.
Peakall, J., K. J. Amos, G. M. Keevil, P. W. Bradbury, and S. Gupta (2007), Flow processes and sedimentation in submarine channel bends, *Mar. Petrol. Geol.*, *24*, 470–486, doi:10.1016/j.marpetgeo.2007.01.008.
Peakall, J., I. A. Kane, D. G. Masson, G. Keevil, W. McCaffrey, and R. Corney (2013), Global (latitudinal) variation in submarine channel sinuosity: Reply, *Geology*, *41*, e288, doi:10.1130/G34319Y.1.
Piper, D. J. W., and W. R. Normark (1983), Turbidite depositional patterns and flow characteristics, Navy Submarine Fan, California Borderland, *Sedimentology*, *30*, 681–694.
Pirmez, C., and J. Imran (2003), Reconstruction of turbidity currents in Amazon Channel, *Mar. Petrol. Geol.*, *20*, 823–849, doi:10.1016/j.marpetgeo.2003.03.005.
Pope, S. B. (2000), *Turbulent Flows*, 771 pp., Cambridge Univ. Press, Cambridge, U. K.
Pyles, D. R., M. Tomasso, and D. C. Jennette (2012), Flow processes and sedimentation associated with erosion and filling of sinuous submarine channels, *Geology*, *40*, 143–146, doi:10.1130/G32740.1.
Richards, K. S. (1982), *Rivers, Form and Process in Alluvial Channels*, 361 pp., Methuen, London.
Rozovskii, I. L. (1957), *Flow of Water in Bends of Open Channels*, 233 pp., Acad. of Sci. of the Ukranian SSR, Kiev (translated from Russian by the Israel Program for Scientific Translations, Jerusalem, 1961).
Seim, H. E., and M. C. Gregg (1997), The importance of aspiration and channel curvature in producing strong vertical mixing over a sill, *J. Geophys. Res.*, *102*, 3451–3472.
Seim, H. E., J. O. Blanton, and S. A. Elston (2009), The effect of secondary circulation on the salt distribution in a sinuous coastal plain estuary: Satilla River, GA, USA, *Cont. Shelf Res.*, 29, 15–28.
Soulsby, R. (1997), *Dynamics of Marine Sands: A Manual for Practical Applications*, 249 pp., Thomas Telford, London.
Stacey, M. W., and A. J. Bowen (1988), The vertical structure of density and turbidity currents – theory and observations, *J. Geophys. Res.*, *93*, 3528–3542.
Sumner, E. J., J. Peakall, D. R. Parsons, R. B. Wynn, S. E. Darby, R. M. Dorrell, S. D. McPhail, J. Perrett, A. Webb, and D. White (2013), First direct measurements of hydraulic jumps in an active submarine density current, *Geophys. Res. Lett.*, *40*, 5904–5908, doi:10.1002/2013GL057862.
Szupiany, R. N., M. L. Amsler, J. L. Best, and D. R. Parsons (2007), Comparison of fixed- and moving-vessel flow measurements with an aDp in a large river, *J. Hydraul. Eng.*, *133*, 1299–1309, doi:10.1061/(ASCE)0733–9429(2007)133:12(1299).
Talling, P. J., D. G. Masson, E. J. Sumner, and G. Malgesini (2012), Subaqueous sediment density flows: Depositional processes and deposit types, *Sedimentology*, *59*, 1937–2003, doi:10.1111/j.1365–3091.2012.01353.x.
Thorne, C. R., L. W. Zevenbergen, J. C. Pitlick, S. Rais, J. B. Bradley, and P. Y. Julien (1985), Direct measurements of secondary currents in a meandering sand-bed river, *Nature*, *315*, 746–747.
Umlauf, L., and L. Arneborg (2009a), Dynamics of rotating shallow gravity currents passing through a channel: Part I: Observation of transverse structure, *J. Phys. Oceanogr.*, *39*, 2385–2401, doi:10.1175/2009JPO4159.1.
Umlauf, L., and L. Arneborg (2009b), Dynamics of rotating shallow gravity currents passing through a channel: Part II: Analysis, *J. Phys. Oceanogr.*, *39*, 2402–2416, doi:10.1175/2009JPO4164.1.
Umlauf, L., L. Arneborg, H. Burchard, V. Fiekas, H. U. Lass, V. Mohrholz, and H. Prandke (2007), Transverse structure of turbulence in a rotating gravity current, *Geophys. Res. Lett.*, *34*, L08601, doi:10.1029/2007GL029521.
UNESCO (1983), Algorithms for computation of fundamental properties of seawater, *UNESCO Tech. Pap. in Mar. Sci. 44*, 53 pp., UNESCO Div. Mar. Sci., Paris.
Wynn, R. B., B. T. Cronin, and J. Peakall (2007), Sinuous deep-water channels: Genesis, geometry and architecture, *Mar. Petrol. Geol.*, *24*, 341–387, doi:10.1016/j.marpetgeo.2007.06.001.
Xu, J. P., and M. A. Noble (2004), In situ measurements of velocity structure within turbidity currents, *Geophys. Res. Lett.*, *31*, L09311, doi:10.1029/2004GL019718.
Xu, J. P., J. P. Barry, and C. K. Paull (2013), Small-scale turbidity currents in a big submarine canyon, *Geology*, *41*, 143–146, doi:10.1130/G33727.1.